Medical Cannabis and Cannabinoids

Research Article

Med Cannabis Cannabinoids 2026;9:163–179
DOI: 10.1159/000552533

Received: December 12, 2025
Accepted: May 7, 2026
Published online: June 1, 2026

# Cannabis Oil Prevents Early Hepatic Fibrosis, Inflammation, and Endothelial Dysfunction in a Sucrose-Rich Diet-Induced MASLD Model: Role of Cannabinoid Receptors

Valentina María Degrave[a] Paola Ingaramo[c] Laura Caltana[d] Daniela Sedan[e] Darío Andrinolo[e] María Eugenia D'Alessandro[a, b] María Eugenia Oliva[a, b]

[a]Laboratorio de Estudio de Enfermedades Metabólicas relacionadas con la Nutrición (LEEMREN). Facultad de Bioquímica y Ciencias Biológicas. Universidad Nacional del Litoral, Santa Fe, Argentina; [b]Consejo Nacional de Investigaciones Científicas y Técnicas (CONICET), Santa Fe, Argentina; [c]Instituto de Salud y Ambiente del Litoral (ISAL), Facultad de Bioquímica y Ciencias Biológicas. Consejo Nacional de Investigaciones Científicas y Técnicas (CONICET), Santa Fe, Argentina; [d]Instituto de Biología Celular y Neurociencias Prof E De Robertis, Facultad de Medicina, Universidad de Buenos Aires, Buenos Aires, Argentina; [e]Centro de Investigaciones del Medio Ambiente (CIM), Consejo Nacional de Investigaciones Científicas y Técnicas (CONICET), Universidad Nacional de La Plata, La Plata, Argentina



**Keywords**
Cannabis oil · Sucrose-rich diet · Liver · Fibrosis · Inflammation · Endothelial dysfunction

**Abstract**

***Introduction:*** Metabolic dysfunction-associated steatotic liver disease (MASLD) is a growing health concern globally, often associated with excessive sugar intake and metabolic dysregulation. In this study, we explored early hepatic alterations induced by a short-term sucrose-rich diet (SRD) and evaluated the preventive effects of a full-spectrum cannabis oil (CO) with a CBD:THC ratio of 2:1. ***Methods:*** Male Wistar rats were assigned to three groups: reference diet, SRD, and SRD plus CO (SRD + CO). CO was administered daily to the SRD + CO group from the onset of SRD exposure and throughout the 3-week experimental period. Liver fibrosis was assessed through hydroxyproline content, total collagen, TGF-β, and CB1R expression. Endothelial dysfunction was evaluated by measuring nitric oxide (NO) levels, endothelial nitric oxide synthase, myeloperoxidase, and VCAM-1 expression. Inflammatory responses were analyzed through hepatic expression of IL-10, TNF-α, PAI-1, MCP-1, F4/80, and CB2R. Transmission electron microscopy was performed on liver tissue to evaluate ultrastructural alterations. ***Results:*** SRD induced significant hepatic fibrosis, endothelial dysfunction, and inflammation. Ultrastructural analysis revealed nuclear alterations, including chromatin condensation, reduced mitochondrial number, intracellular lipid accumulation, increased glycogen deposits, and stromal changes characterized by perisinusoidal and periportal fibrosis with inflammatory cell infiltration. CO administration attenuated these pathological features and was accompanied by modulation of cannabinoid receptor expression. ***Conclusion:***

karger@karger.com
www.karger.com/mca



Correspondence to:
M.E. Oliva, meoliva@fbcb.unl.edu.ar

These findings highlight the preventive effects of CBD- and THC-containing CO against early liver alterations associated with MASLD.


## Introduction

Metabolic dysfunction-associated steatotic liver disease (MASLD), formerly known as non-alcoholic fatty liver disease, is currently the most common liver disease worldwide. It encompasses a spectrum of liver pathologies, progressing from simple steatosis to steatohepatitis, fibrosis, cirrhosis, and, ultimately, hepatocellular carcinoma. MASLD is intimately associated with components of the metabolic syndrome, including central obesity, insulin resistance, hypertension, and dyslipidemia [1, 2].

Dietary patterns characterized by high intake of refined carbohydrates, particularly sucrose and fructose, have been strongly implicated in the development of hepatic steatosis and its progression toward more severe forms of liver damage [3]. Experimental models based on a sucrose-rich diet (SRD) in rats have demonstrated that short-term administration can induce key features of MASLD, including hepatic lipid accumulation, inflammation, oxidative stress, and the early activation of fibrogenic pathways. These pathological processes are mediated by a complex interplay of metabolic stress, mitochondrial dysfunction, and immune cell infiltration within the liver [4, 5].

Hepatic fibrosis, a hallmark of MASLD progression, is characterized by the excessive deposition of extracellular matrix (ECM), primarily driven by the activation of hepatic stellate cells (HSCs) and the upregulation of profibrotic cytokines such as transforming growth factor-beta (TGF-β) [6, 7]. In preclinical models, the quantification of hydroxyproline content and collagen accumulation are commonly employed as reliable indicators of fibrosis severity [8–11]. Another key pathological feature of MASLD is endothelial dysfunction, involving reduced nitric oxide (NO) bioavailability, increased expression of vascular adhesion molecules such as VCAM-1, and elevated myeloperoxidase (MPO) activity. These factors collectively contribute to a systemic proinflammatory and proatherogenic environment [12, 13]. Concurrently, hepatic inflammation plays a pivotal role in disease progression, characterized by elevated levels of proinflammatory cytokines such as tumor necrosis factor-alpha (TNF-α) and interleukin-6 (IL-6) and chemokines like monocyte chemoattractant protein-1 (MCP-1), and macrophage infiltration markers such as F4/80. Additionally, the expression of plasminogen activator inhibitor-1 (PAI-1) reflects the interplay between inflammation and fibrogenesis. Notably, reduced levels of the anti-inflammatory cytokine interleukin-10 (IL-10) further exacerbate the imbalance of immune responses in MASLD [14–16].

Recent research has focused on the endocannabinoid system (ECS) as a key regulatory network implicated in energy homeostasis, immune modulation, and liver pathophysiology. The cannabinoid receptor 1 ($CB_1R$), which is expressed in hepatocytes and HSCs, is known to promote steatosis, fibrogenesis, and inflammation upon overactivation. Conversely, cannabinoid receptor 2 ($CB_2R$), which is predominantly expressed in immune cells, exerts documented anti-inflammatory and potentially antifibrotic effects. These opposing receptors functions suggest that selective modulation of the ECS could offer a promising therapeutic avenue for MASLD [17–19].

Phytocannabinoids, such as cannabidiol (CBD) and Δ9-tetrahydrocannabinol (THC), interact with the ECS and various other signaling pathways, providing antioxidant, anti-inflammatory, and antifibrotic properties. Full-spectrum cannabis extracts, which combine phytocannabinoids like CBD and THC, have emerged as therapeutic candidates in preclinical studies for the treatment of liver disorders associated with metabolic dysfunction [20, 21]. Previous studies conducted by our group have demonstrated hepatoprotective and antioxidant effects following the administration of full-spectrum COs in rats fed an SRD for 3 weeks [5, 22]. However, the evidence concerning their efficacy during the early stages of MASLD, and specifically their impact on key pathological features such as hepatic fibrosis, inflammation, and endothelial function remains highly limited.

In the present study, we investigated the effects of a full-spectrum CO (CBD:THC 2:1 ratio) on liver fibrosis, endothelial dysfunction, inflammation, and the regulation of the ECS in a SRD-induced MASLD model. Specifically, we assessed key molecular markers related to fibrosis (hydroxyproline, TGF-β, collagen content), endothelial stress (NO, eNOS, MPO, VCAM-1), and inflammation (IL-10, TNF-α, F4/80, MCP-1, PAI-1). Furthermore, we analyzed the expression of $CB_1R$ and $CB_2R$, central components of the ECS. Additionally, TEM was employed to characterize ultrastructural hepatic changes during the early phase of MASLD.

## Methods

*Cannabis Oil Preparation and Characterization*

Cannabis oil was obtained from dried inflorescences of the *Cannabis sativa* CAT1 variety grown at the Environmental Research Center (CIM-CONICET-UNLP) (RESOL-2021-3236-APN-MS), as previously described by Degrave et al. [5]. Finally, adequate dilution was performed to obtain the working oil at a concentration of 1 mg/mL.

*Animals and Diets*

Male Wistar rats ($n$ = 18) were purchased from the Veterinary Sciences Institute of Litoral (ICIVET-Litoral) – Faculty of Veterinary Sciences, National University of Litoral (Esperanza, Santa Fe, Argentine), and were maintained with unrestricted access to water and food under controlled temperature (22 ± 1°C), humidity, and air flow conditions, with a fixed 12-h light/dark cycle (light on 07.00 AM – 07.00 PM). Adequate measures were taken to minimize pain or discomfort in the rats, and the smallest number of animals possible was used. This study was performed in strict accordance with the NIH guidelines for the care and use of laboratory animals and approved by the Institutional Ethics Committee of the Faculty of Biochemistry and Biological Sciences (UNL, Santa Fe, Argentine – Acta 03/21).

The animals were initially fed a standard powdered commercial rodent diet (GEPSA FEED, Buenos Aires, Argentine). Rat's weight was 180–190 g (young adults) and were randomly assigned to the following three experimental groups at study initiation, while maintaining comparable initial body weights among groups: (1) rats fed a standard powdered rodent commercial diet (reference diet, RD, $n$ = 6); (2) rats fed a semisynthetic SRD ($n$ = 6); (3) rats fed an SRD plus orally administered CO (SRD + CO, $n$ = 6). Rats received noninvasive oral CO (CBD:THC, 2:1 ratio; SRD + CO) or vehicle control (corn oil; RD and SRD). CO was administered at a dose of 1 mg/kg body weight daily, simultaneously with the initiation of the SRD, and was maintained during the experimental protocol (3 weeks). The diet compositions are detailed in a study by Degrave et al. [22]. Individual body weight was recorded daily. Food intake of the animals in each group were assessed twice a week throughout the experimental period. At the end, the food was removed at 07.00 AM and experiments were performed between 07.00 and 09.00 AM. Animals were anesthetized with intraperitoneal sodium pentobarbital (60 mg/kg body weight). Blood samples were collected from the inferior vena cava and rapidly centrifuged, and serum was either immediately assayed or stored at −20°C until use. The liver of each rat was totally removed, weighed, and sectioned for different subsequent assays. Liver samples were fixed in 10% (v/v) buffered formalin for 24 h at room temperature and embedded in paraffin for immunohistochemistry (IHC) analysis, fixed with 4% w/v paraformaldehyde and 0.25% v/v glutaraldehyde for TEM, or frozen and stored at the temperature of liquid $N_2$. The animals were euthanized by removal of a vital organ (heart). Outcome assessments were performed according to standardized procedures, and image-based analyses were conducted in a blinded manner whenever feasible.

*Analytical Methods*

Serum glucose, uric acid, triglyceride, and total cholesterol levels were measured by spectrophotometric methods using commercial enzymatic kits according to the manufacturer's protocols (Wiener Lab., Argentina). Serum activities of aspartate aminotransferase (AST), alanine aminotransferase (ALT), and alkaline phosphatase (AP) enzymes were measured by spectrophotometric methods using commercial enzymatic kits according to the manufacturer's protocols (Wiener Lab., Argentina). Liver triglyceride content was determined according to Hein et al. [23].

*Hydroxyproline Analysis*

Hydroxyproline content in the liver was measured according to Neuman and Logan [24], with slight modifications as previously described [25].

*Tissue Histology*

For histological examination, paraffin sections (5 μm) of liver samples were cut and stained with Sirius Red (Direct Red 80, Sigma-Aldrich, Argentina) in picric acid solution (picrosirius) counterstained with Harris hematoxylin. The liver structure and collagen organization were evaluated using Olympus BH2 light microscopy (Olympus Optical Co., Ltd., Japan) [26]. In addition, the collagen birefringence of picrosirius-stained liver samples was quantified by polarization microscopy. At least 10 fields per section of each animal were assessed. The area occupied by organized collagen was measured using Image Pro-Plus 4.1.0.1® system (Media Cybernetics, Silver Spring, USA). Images were recorded with a Spot Insight V3.5 color video camera attached to an Olympus BH2 microscope and converted to gray scale. The hepatic collagen content was determined by calculating the birefringent area and expressing it as a percentage of the total image area [27].

*Nitric Oxide, NOS, and MPO Enzymatic Activity*

Nitric oxide (NO) levels and nitric oxide synthase (NOS) enzymatic activity were measured in both serum and liver samples, while MPO activity was assessed exclusively in liver tissue. All measurements were performed according to the protocols described by Vega Joubert et al. [27], which adapt established spectrophotometric methods specific for each assay.

*Immunohistochemical Analysis*

A standard IHC technique, following protocols previously described [27, 28], was performed. Paraffin-embedded (5 μm thickness) liver cross-sections were used to evaluate the protein expression of TGF-β, VCAM-1, F4/80, $CB_1R$, $CB_2R$, and alpha smooth muscle actin (α-SMA). The sections were mounted on 3-aminopropyltriethoxysilane (Sigma-Aldrich, Argentine)-coated slides and a subsequent microwave pretreatment for antigen retrieval was performed. The samples were incubated in a humid chamber first with a specific primary antibody for TGF-β, VCAM-1, F4/80, $CB_1R$, and $CB_2R$ (for 14–16 h at 4°C) and then with biotin-conjugated secondary antibody (anti-mouse, 1: 100 dilution, Sigma-Aldrich, Argentina) for 30 min at room temperature. The reactions were developed using the streptavidin-biotin peroxidase method and diaminobenzidine (Sigma Aldrich, Argentina) as a chromogenic substrate. Each immune-histochemical run included positive and negative controls. In situ protein co-localization was performed by double immunohistochemistry. After visualization of $CB_1R$ and $CB_2R$ expression with diaminobenzidine (brown staining), tissue sections were rinsed in PBS and subjected to a second IHC to detect a different protein (α-SMA or F4/80). The reaction was developed using $NiCl_2$ as a diaminobenzidine intensifier, yielding a black signal. Thus, the distinct staining colors in these double-labeling assays allow the identification of co-expression of two proteins within the same cell. The expression of TGF-β, VCAM-1, and F4/80 was evaluated by image analysis using the Image Pro-Plus 5.0.2.9 system (Media Cybernetics, Silver Spring, MD, USA). Immunostained images were captured with a Dplan 40× objective (numerical aperture, 0.65; Olympus) attached to a Spot Insight V3.5 color video camera. Quantification was performed on at least 10 randomly selected fields per section. After converting each image into a gray scale, the integrated optical density was measured as a linear combination of the average gray intensity and the relative area occupied by positive cells as was previously described by Ingaramo et al. [29].

*Real-Time PCR for TGF-β, TNFα, IL-1, PAI-1, and MCP-1 mRNA Expression Quantitation*

TGF-β, TNFα, IL-10, PAI-1, and MCP-1 mRNA levels were determined by semiquantitative RT-PCR analysis following protocols of Ingaramo et al. [28]. The total RNA was obtained from tissue samples using the TRIzol reagent (TRI Reagent®, Sigma Aldrich, USA) according to the manufacturer's instructions. The concentration and purity of total RNA were determined by measuring absorbance at 260 and 280 nm using a NanoDrop™ Lite Spectrophotometer (Thermo Fisher Scientific). Total RNA (1 μg) was reverse transcribed into cDNA with Moloney murine leukemia virus reverse transcriptase (Promega, Madison, WI, USA), using random primers (Biodynamics SRL) and deoxynucleotide triphosphate. Reverse transcription was performed at 37°C for 90 min and at 42°C for 15 min. Reactions were stopped by heating at 80°C for 5 min and cooling on ice. Each reverse-transcribed product was diluted with ribonuclease-free water to a final volume of 60 μL and further amplified using the realtime StepOne system (Thermo Fisher scientific, Buenos Aires, Argentina). L19 was used as a housekeeping gene. For cDNA amplification, 5 μL of cDNA was combined with SsoFastTM EvaGreen® Supermix (Bio Rad) and 10 pmol of each primer (Genbiotech) in a final volume of 20 μL. The primers employed are listed in Table 1. After the initial denaturation at 95°C for 15 min, the reaction mixture was subjected to successive cycles of denaturation at 95°C for 15 s, annealing for 15 s at 60°C, and extension at 72°C for 15 s. Controls containing no template DNA were included in all assays, yielding no consistent amplification. For each sample, cycle threshold (CT) was calculated as the difference in CT between target mRNA and L19 mRNA. The CT for each sample was calculated using the software StepOne (ThermoFisher scientific, Buenos Aires, Argentina). For all experimental samples, the relative target quantity was determined from the standard curve, normalized to the relative quantity of the reference gene and finally divided by the normalized target value of the control sample. No significant differences in CT values were observed for the ribosomal protein L19 between the different experimental groups.

*Western Blot Analysis*

Frozen liver samples were homogenized in a RIPA buffer supplemented with protease inhibitors, left on ice for 10 min, and the supernatant was collected by centrifugation at 25,000×g for 10 min, as described by Li et al. [30]. Proteins were separated by SDS-PAGE in a 10% gel and electrotransferred onto PVDF membranes. The membranes were probed with mouse primary monoclonal antibodies against $CB_1R$ and $CB_2R$ (mouse monoclonal antibody; sc-518035 and sc-293188, Santa

**Table 1.** qPCR primers sequences

| Name | Forward sequences | Reverse sequences |
|---|---|---|
| L19 | AGCCTGTGACTGTCCATTCC | TGGCAGTACCCTTCCTCTTC |
| TNF-α | CATTCACCAGCGTTGCC | CATCAGCAGAGCCAGGA |
| PAI-1 | AGGGCTTCATGCCCCACTTCTTCA | AGTAGAGGGCATTCACCAGCACCA |
| IL-10 | ACACACAATGGAAGAATCAA | CTCAGTTACCCAAAGGAAAC |
| MCP-1 | GGTTTTTCCACACTGGGCAAC | GGTAACCTGTTGAGAGGGCAA |

Cruz Biotechnology) and then incubated with goat anti-mouse IgG conjugated to horseradish peroxidase antibody (mIgG-Fc-BP-HRP; sc-525409, Santa Cruz Biotechnology). Specific signals were visualized using a chemiluminescent detection system (Bio-Lumina, Productos Bio-Logicos, Argentina) according to the manufacturer's instructions. The intensity of the bands was quantified using optical densitometry (Scion Image Release Beta 4.0.2, NIH, USA). After densitometry of immunoblots, values of the RD group were normalized to 100%, and both SRD and SRD + CO were expressed relative to this. The protein levels were normalized to those of β-actin.

*Transmission Electron Microscopy*

Dissected sections of liver were fixed with 4% w/v paraformaldehyde and 0.25% v/v glutaraldehyde. After 4 h, samples were post-fixed in 1% w/v osmium tetroxide for 30 min. After dehydration in an ethanol gradient, samples were contrasted with 5% w/v uranyl acetate and embedded in Durcupan (Fluka AG Chemische Fabrik, Buchs, SG, Switzerland). Ultrathin sections were obtained with a Reichert-Jung Ultracut E ultramicrotome (Leica Microsystems GmbH, Wetzlar, Germany) and stained with lead citrate [31]. Images were acquired on a Zeiss 109 Transmission Electron Microscope (TEM) (Carl Zeiss, Oberkochen, Germany) and photographed with a Gatan CCD camera (Pleasanton, CA, USA).

*Statistical Analysis*

Results were expressed as mean ± SEM. Statistical comparisons were made transversely between different dietary groups. Data were tested for variance using Levene's test and normality by Shapiro-Wilk's test. The statistical difference between groups (RD, SRD, and SRD + CO) was determined by one-way ANOVA followed by post hoc Newman-Keuls' test. $p$ values lower than 0.05 were considered to be statistically significant (SPSS 17.0 for Windows, SPSS INC. Chicago, Illinois).

## Results

Considering that CO administration occurred concomitantly with SRD exposure, the present findings should be interpreted within a preventive context.

*General, Metabolic, and Hepatic Parameters*

As we previously reported [22], SRD-fed rats develop characteristic metabolic alterations, including significant increases in serum uric acid, triglycerides, and total cholesterol, together with elevated hepatic enzyme activities, which are indicative of dyslipidemia and early hepatocellular injury. Likewise, and as described earlier, SRD feeding induces a marked accumulation of hepatic triglycerides, reflecting the early establishment of steatosis. These findings, already documented by our group, were reproduced in the present study, confirming the robustness of the MASLD model. Similarly, and in agreement with our previous reports, no significant differences in body weight or food intake were observed among groups, indicating that the metabolic and hepatic alterations depend on the type of diet rather than on differences in food consumption or weight gain. In this context, CO administration significantly attenuated these metabolic and hepatic disturbances: it reduced circulating uric acid and lipid levels, normalized liver enzyme activities toward RD-fed values, and partially decreased hepatic triglyceride accumulation. No significant differences in serum glucose levels were detected among the groups (Table 2).

*Liver Fibrosis Markers and $CB_1R$ Expression*

SRD-fed rats exhibited clear indicators of early hepatic fibrogenesis (Fig. 1). Compared with the RD group, the SRD group showed significant increase in hepatic collagen content, elevated hydroxyproline levels, and up-regulated TGF-β expression ($p < 0.0001$). $CB_1R$ expression was also significantly higher in the SRD group.

CO administration markedly attenuated these profibrotic changes, resulting in a significant reduction in

**Table 2.** SRD altered serum metabolic parameters, liver damage enzymes, and hepatic triglyceride content, while daily CO administration attenuated most of these changes without affecting body weight or food intake

| | RD | SRD | SRD + CO | *p* value |
|---|---|---|---|---|
| Initial body weight, g | 178.0±2.5 | 180.3±4.3 | 179.7±2.3 | **0.1262** |
| Final body weight, g | 269.92±4.85 | 267.3±5.9 | 272.2±4.1 | **0.2702** |
| Food intake, g/day | 16.82±0.35 | 16.87±0.27 | 16.90±0.43 | **0.9851** |
| *Serum metabolites* | | | | |
| Glucose, mM | 8.51±0.15 | 8.44±0.16 | 8.42±0.19 | **0.1705** |
| Uric acid, μM | 63.97±6.12$^{b}$ | 120.30±6.07$^{a}$ | 77.55±3.75$^{b}$ | <**0.0001** |
| Triglyceride, mM | 1.32±0.09$^{b}$ | 3.08±0.16$^{a}$ | 1.23±0.07$^{b}$ | <**0.0001** |
| Total cholesterol, mM | 2.02±0.10$^{b}$ | 2.64±0.09$^{a}$ | 2.12±0.18$^{b}$ | <**0.0001** |
| *Liver damage enzymes* | | | | |
| AST, U/L | 19.56±0.75$^{b}$ | 27.31±0.82$^{a}$ | 21.54±1.35$^{b}$ | **0.0002** |
| ALT, U/L | 20.93±1.39$^{b}$ | 29.92±0.73$^{a}$ | 21.57±1.97$^{b}$ | <**0.0001** |
| AP, U/L | 672.42±54.61$^{c}$ | 1,183.01±25.07$^{a}$ | 1,032.03±11.95$^{b}$ | <**0.0001** |
| *Liver lipids* | | | | |
| Triglycerides, μmol/g WT | 7.53±0.79$^{c}$ | 14.48±0.98$^{a}$ | 10.15±0.84$^{b}$ | <**0.0001** |

Values are expressed as mean ± SEM, $n = 6$. The $p$ values shown in the last column correspond to the global comparison among groups by one-way ANOVA. Values in a line that do not share the same superscript letter are significantly different ($p < 0.05$) according to the Newman-Keuls post hoc test. RD, SRD, or SRD + CO. WT, wet tissue.

collagen accumulation, hydroxyproline content, and TGF-β expression ($p < 0.0001$). Hepatic $CB_1R$ levels were normalized to control values. These findings demonstrate that CO treatment effectively counteracted the profibrotic activation induced by SRD feeding.

*Markers of Endothelial Activation*

As shown in Table 3, SRD-fed rats displayed significantly elevated serum and hepatic nitric oxide (NO) levels, increased NOS activity, and higher MPO activity compared with RD-fed rats ($p < 0.05$). This profile is indicative of enhanced nitrosative stress and endothelial inflammatory activation. CO administration significantly reduced NO production, NOS activity, and MPO levels ($p < 0.05$), restoring these parameters toward RD values.

VCAM-1 IHC corroborated these biochemical findings (Fig. 2). Liver sections from the SRD group exhibited intense VCAM-1 staining, suggestive of marked endothelial activation and inflammatory cell recruitment. In contrast, SRD + CO group showed markedly reduced VCAM-1 immunoreactivity, comparable to the RD group.

*Hepatic Cytokines and $CB_2R$ Expression*

SRD-fed rats exhibited a pronounced hepatic inflammatory response (Fig. 3). The levels of proinflammatory markers such as TNF-α, MCP-1, PAI-1, and F4/80 were significantly increased compared with the RD group ($p < 0.05$). Conversely, the anti-inflammatory cytokine IL-10 was significantly decreased, indicating a clear shift toward a pro-inflammatory microenvironment. In parallel, hepatic $CB_2R$ expression was significantly increased in the SRD group, suggesting an adaptive immunomodulatory response to diet-induced inflammation.

CO administration effectively prevented these alterations, reducing TNF-α, MCP-1, PAI-1, and F4/80 levels ($p < 0.05$) while simultaneously increasing IL-10 expression. Moreover, $CB_2R$ expression returned to control values in the SRD + CO group, supporting the immunomodulatory effects of CO.

*Cellular Localization of Cannabinoid Receptors*

To further explore the cellular localization of cannabinoid receptors, double-labeling immunohistochemistry was performed (Fig. 4). $CB_1R$ staining was

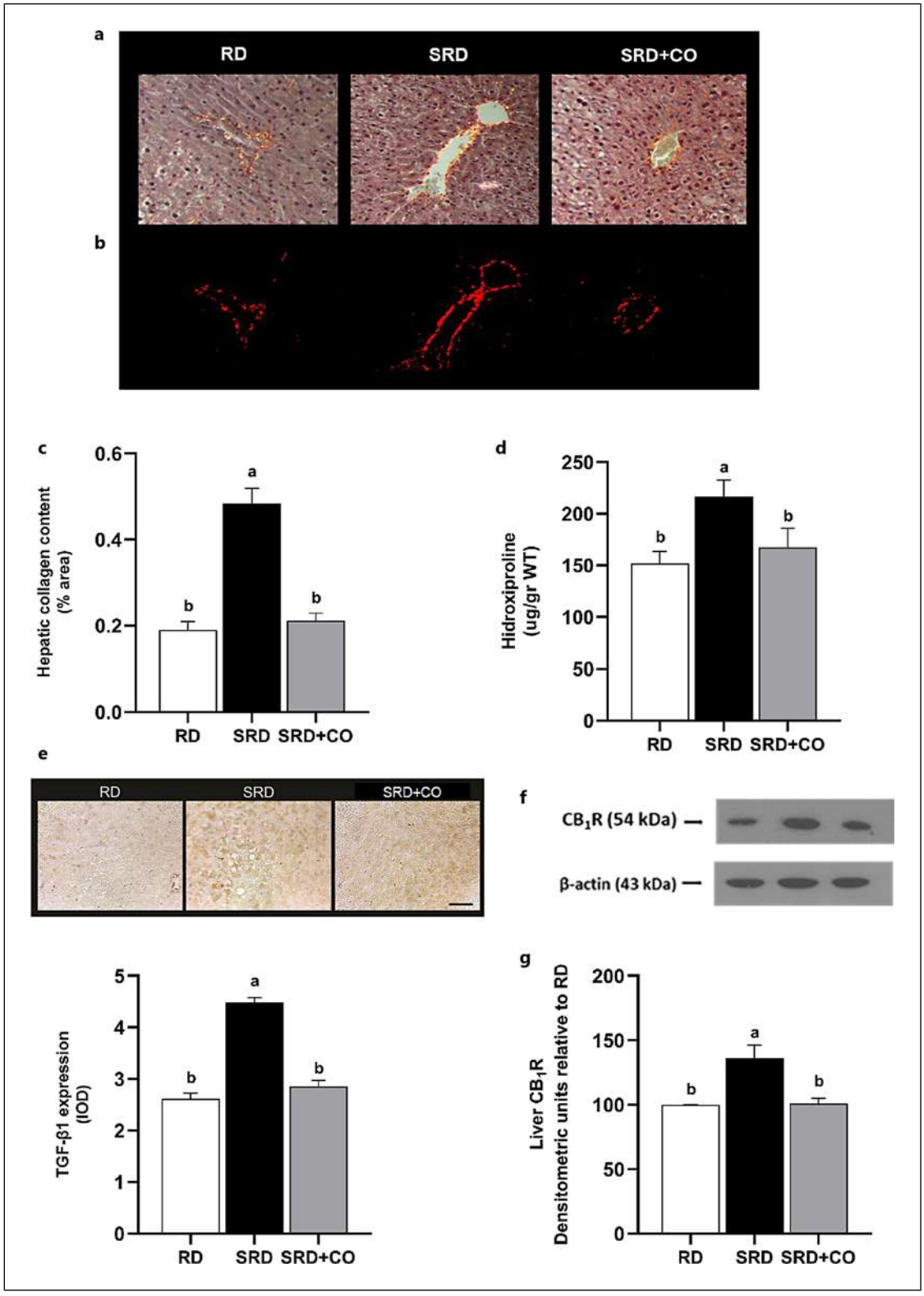


1

*(For legend see next page.)*

increased in SRD animals and showed partial co-localization with α-actin-positive cells, suggesting its association with activated HSCs (Fig. 4a). In contrast, $CB_2R$ expression was also elevated in SRD livers and partially co-localized with F4/80-positive cells, although macrophage presence was limited in this early-stage model (Fig. 4b). CO treatment attenuated both $CB_1R$ and $CB_2R$ immunoreactivity, consistent with its anti-fibrotic and anti-inflammatory effects.

*Hepatic Ultrastructure (TEM)*

In RD-fed rats, hepatocytes exhibited normal ultrastructural organization. Nuclei showed smooth contours with evenly distributed euchromatin and well-defined nucleoli. Mitochondria were abundant and preserved. The cytoplasm presented minimal lipid droplets and sparse glycogen granules and the stroma displayed a regular architecture.

TEM revealed marked ultrastructural alterations in SRD-fed rats (Fig. 5). Hepatocytes exhibited nuclear irregularities with chromatin condensation, reduced mitochondrial content, intracellular lipid droplet accumulation, and increased glycogen deposits. The hepatic stroma showed perisinusoidal and periportal fibrosis accompanied by inflammatory cell infiltration, indicating early microarchitectural disruption.

CO administration prevented these alterations. Hepatocytes displayed preserved nuclear morphology, reduced lipid and glycogen accumulation, and improved mitochondrial appearance, indicating a protective effect on cellular homeostasis. Furthermore, the hepatic stroma showed no evidence of fibrosis or inflammatory infiltration.

## Discussion

The present study demonstrates that 3 weeks of SRD exposure are sufficient to induce a constellation of hepatic alterations characteristic of the early stages of MASLD. These include initial fibrosis, inflammatory activation, endothelial dysfunction, and pronounced ultrastructural damage. Collectively, our findings reveal the high sensitivity of the liver to short-term refined carbohydrate excess and underscore the urgent need for strategies aimed at reducing simple sugar consumption.

SRD-fed rats exhibited a significant profibrotic response, evidenced by increased collagen content, elevated hydroxyproline levels, and upregulated TGF-β expression, accompanied by marked $CB_1R$ overexpression. Together, these alterations indicate that even brief sucrose exposure rapidly activates fibrogenic mechanisms, most likely through early HSC stimulation and enhanced ECM deposition. TGF-β is a well-established driver of fibrosis [7], while $CB_1R$ signaling promotes HSC activation, collagen synthesis, and metabolic dysregulation [17, 19]. Recent evidence supports the central role of $CB_1R$ in diet-induced liver injury, showing that $CB_1R$ stimulation accelerates fibrogenesis and lipid accumulation, whereas its inhibition attenuates ECM expansion and favors hepatic remodeling [32]. Our results therefore support the concept that excess sucrose rapidly engages TGF-β- and $CB_1R$-dependent profibrotic pathways during early MASLD development [13].

SRD feeding also triggered a pronounced inflammatory response, as shown by elevated TNF-α, MCP-1, PAI-1, and the macrophage marker F4/80, along with decreased IL-10 levels. This profile reflects an early proinflammatory shift driven by immune cell recruitment and Kupffer cell activation, in line with previous findings [14, 33–36]. Moreover, the inflammatory profile observed in SRD-fed rats is consistent with the emerging concept of metainflammation, a nutrient-induced, low-grade inflammatory state tightly linked to metabolic stress. Metainflammation arises when chronic nutrient overload activates innate immune pathways – particularly TNF-α- and MCP-1-driven cascades – leading to persistent immune cell recruitment, altered cytokine profiles, and early tissue remodeling. The increase in proinflammatory mediators together with reduced IL-10 observed here is characteristic of this metabolic inflammatory state and provides mechanistic insight into how short-term sucrose excess rapidly

**Fig. 1.** SRD increased liver fibrosis markers and $CB_1R$ protein levels, while daily cannabis oil administration prevented these alterations. **a** Picrosirius-stained histological sections of liver. Abnormal collagen deposition is observed around hepatocytes and blood vessels in the SRD group. **b** Polarized light. Scale bar: 50 $\mu$m. **c** Quantification of collagen-positive areas was calculated relative to the total areas in liver sections. **d** Hydroxyproline content of liver. **e** Representative photomicrographs and quantitative immunohistochemical analysis of expression of TGF-β1 ($p < 0.0001$). Scale bar: 50 $\mu$m. Values (mean ± SEM, $n = 6$) are expressed as integrated optical density (IOD). **f** Representative immunoblot of liver $CB_1R$ receptor. Each gel contained an equal number of samples from rats fed an RD, SRD, and SRD + CO. Values are expressed as mean ± SEM ($n = 6$). **g** Liver $CB_1R$ receptor protein mass ($p = 0.0063$). Bars that do not share the same letter are significantly different ($p < 0.05$) by one-way ANOVA followed by the Newman-Keuls test.

**Table 3.** SRD induced serum and hepatic alterations in nitric oxide-related parameters and MPO levels, which were prevented by daily cannabis oil administration

| | RD | SRD | SRD+CO | *p* value |
|---|---|---|---|---|
| Serum NO, *η*mol/L | 18.69±3.61[b] | 49.28±6.71[a] | 19.41±4.27[b] | **0.0015** |
| Liver NO, *η*mol/g WT | 49.36±8.26[b] | 164.2±43.41[a] | 56.60±11.08[b] | **0.0027** |
| Serum NO synthase, U/L | 68.79±8.99[b] | 156.62±12.01[a] | 73.10±15.69[b] | <**0.0001** |
| Liver NO synthase, U/mg protein | 3.98±1.25[b] | 13.77±2.78[a] | 4.73±1.03[b] | **0.0002** |
| MPO, mU/mg protein | 32.44±3.95[b] | 78.38±8.14[a] | 42.34±3.97[b] | **0.0005** |

Values are expressed as mean ± SEM, $n = 6$. The $p$ values shown in the last column correspond to the global comparison among groups by one-way ANOVA. Values in a line that do not share the same superscript letter are significantly different ($p < 0.05$) according to the Newman-Keuls post hoc test. RD, SRD, or SRD + CO. WT, wet tissue.

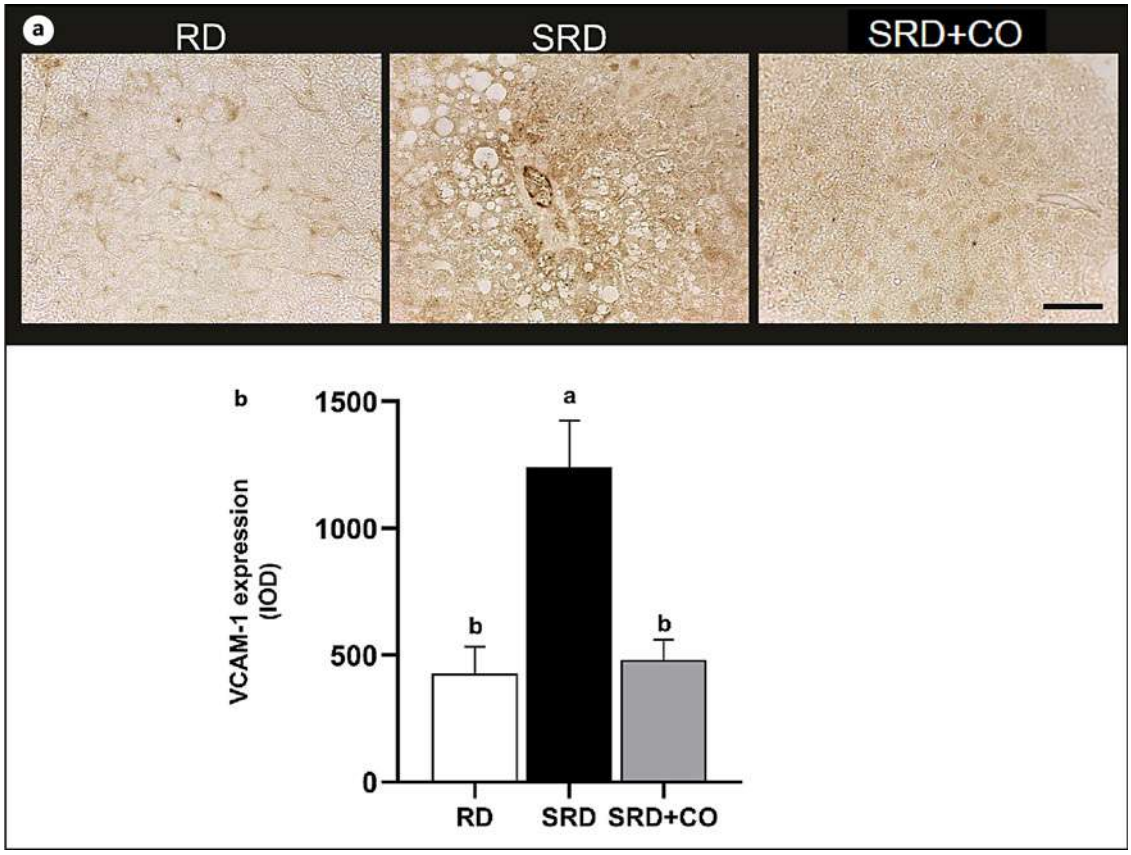


**Fig. 2.** SRD increased hepatic VCAM-1 expression, while daily cannabis oil administration prevented this alteration. **a** Microscopic analysis of liver immunocytochemical staining. Magnification of ×400 shows positive marks around lipid droplets in the SRD group. Scale bar: 50 $\mu$m. **b** Quantitative immunohistochemical analysis of VCAM-1 expression. Values (mean ± SEM, $n = 6$) are expressed as integrated optical density (IOD) ($p = 0.0050$). Values are expressed as mean ± SEM ($n = 6$). Bars that do not share the same letter are significantly different ($p < 0.05$) by one-way ANOVA followed by the Newman-Keuls test.

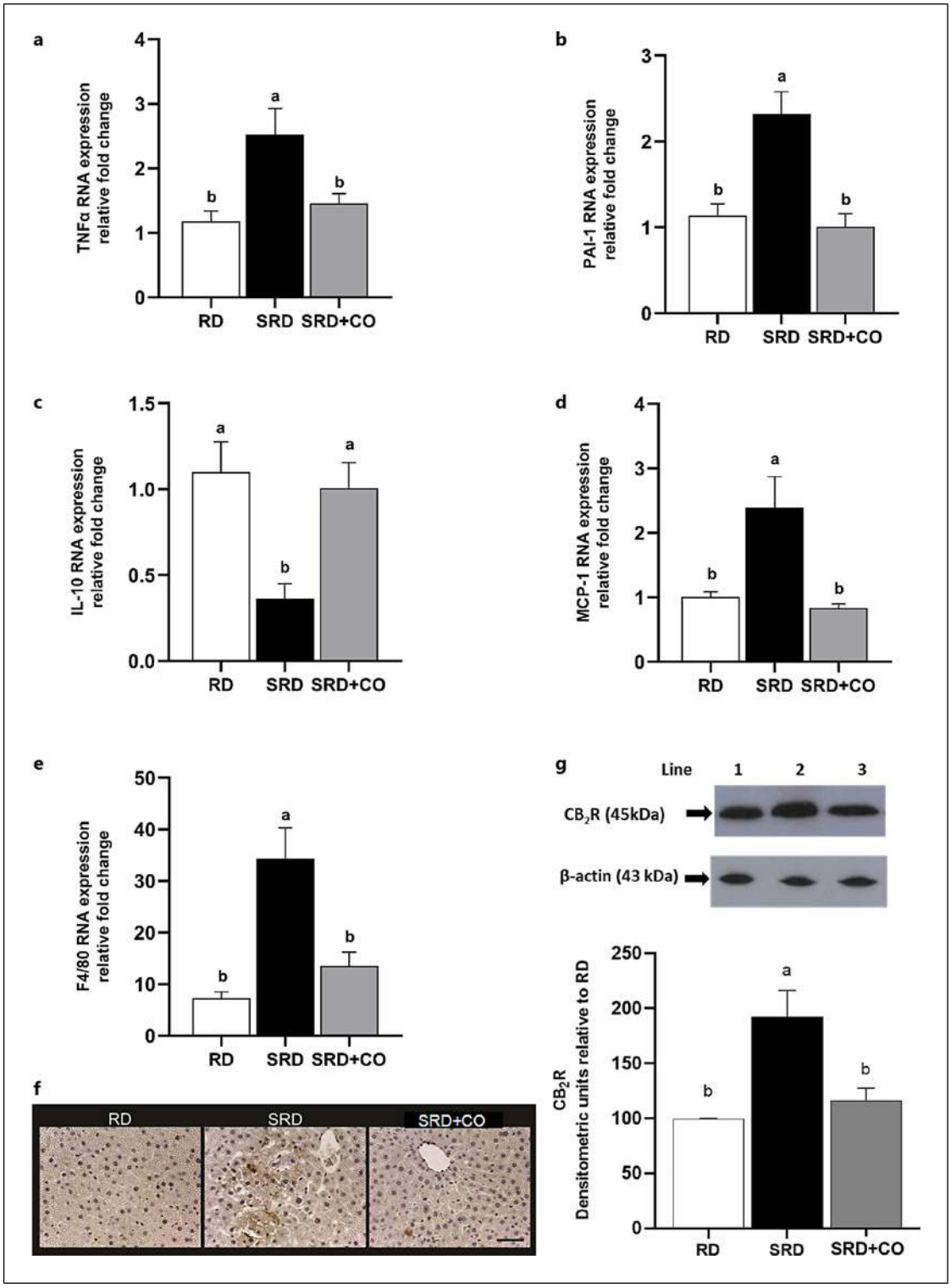


3

*(For legend see next page.)*

shifts the liver toward a proinjury environment that predisposes to fibrosis and endothelial dysfunction [37–39].

In this context, the observed upregulation of hepatic $CB_2R$ in SRD-fed rats may represent an adaptive counter-regulatory response of the ECS. $CB_2R$ activation limits macrophage recruitment, decreases cytokine release, and reduces tissue injury [40, 41] promoting a shift toward a less inflammatory macrophage phenotype. Thus, $CB_2R$ upregulation likely reflects an intrinsic attempt to mitigate sucrose-induced inflammatory stress.

SRD-fed animals exhibited clear signs of endothelial dysfunction, including increased NO levels, enhanced NOS activity, elevated MPO, and upregulated VCAM-1 expression. This pattern indicates early endothelial and neutrophil activation and disruption of the hepatic sinusoidal microenvironment. These findings align with studies highlighting endothelial dysfunction as a key early driver of MASLD progression [42, 43]. In particular, VCAM-1 upregulation in liver sinusoidal endothelial cells facilitates leukocyte adhesion and fibrogenic progression and its inhibition reduces hepatic fibrosis [44]. Our data therefore position endothelial alterations – especially dysregulated NO production, enhanced MPO activity, and increased VCAM-1 – as fundamental early mechanisms linking metabolic overload with inflammation and fibrogenesis.

TEM analyses provided direct visualization of early metabolic and structural deterioration. SRD-fed animals exhibited chromatin condensation, reduced mitochondrial number, lipid droplet accumulation, glycogen overload, and stromal fibrosis with inflammatory infiltrates – hallmarks of early MASLD. The presence of stromal fibrosis after 3 weeks is particularly notable and corresponds with biochemical evidence of increased collagen and TGF-β. These alterations match recent reports demonstrating that ECM remodeling and TGF-β-mediated profibrotic signaling are activated rapidly following metabolic insults [45]. Moreover, early liver sinusoidal endothelial cell dysfunction – characterized by capillarization and increased inflammatory mediators – facilitates HSC activation and accelerates fibrosis [13]. Collectively, these observations confirm that short-term SRD exposure triggers rapid fibrogenic mechanisms via coordinated endothelial, inflammatory, mitochondrial, and HSC-related processes.

Administration of the CBD:THC 2:1 full-spectrum CO markedly attenuated SRD-induced hepatic inflammation, as reflected by reductions in TNF-α, MCP-1, PAI-1, and F4/80-positive macrophages, accompanied by restored IL-10 levels and normalization of $CB_2R$ expression. This profile is consistent with robust $CB_2R$-mediated anti-inflammatory effects described in experimental models [40, 46–49]. These results support the concept that phytocannabinoids combinations exert potent anti-inflammatory actions by enhancing $CB_2R$ expression and the attenuation of $CB_1R$ upregulation, consistent with previous evidence linking these receptors to inflammatory and fibrogenic pathways.

CBD:THC 2:1 CO also significantly reduced collagen deposition, hydroxyproline levels, and TGF-β and $CB_1R$ expression, suggesting mitigation of early HSC activation and ECM expansion. These findings are consistent with earlier studies showing that cannabinoids – particularly CBD-rich formulations – attenuate fibrogenesis by inhibiting $CB_1R$-dependent pathways and TGF-β/Smad signaling [46, 47, 50]. $CB_1R$ antagonism has similarly been shown to restore mitochondrial activity and reduce fibrosis [51], aligning with the hepatoprotective effects observed here.

Treatment with the CO partially reversed SRD-induced endothelial dysfunction, reducing NO production, MPO activity, and VCAM-1 expression. These protective effects are supported by studies demonstrating that CBD reduces adhesion molecule expression and oxidative/nitrative stress in endothelial cells [52] and prevents high-glucose-induced VCAM-1 and ICAM-1 upregulation [53]. Additional evidence from peripheral vasculature supports CBD-mediated improvements in eNOS activity and endothelial homeostasis [54].

TEM analyses showed that CBD:THC 2:1 CO preserved hepatocyte architecture, reducing lipid droplets, glycogen accumulation, mitochondrial alterations, and

**Fig. 3.** RD increased hepatic inflammatory markers, macrophage infiltration, and $CB_2R$ protein levels, while daily cannabis oil administration prevented these alterations. **a–d** Hepatic mRNA expression levels of TNF-α ($p = 0.0046$), PAI-1 ($p = 0.0004$), IL-10 ($p = 0.0016$), and MCP-1 ($p = 0.0027$) in liver. **e** Quantitative immunohistochemical analysis of F4/80 expression in liver. **f** Representative photomicrographs of immunocytochemical staining F4/80 ($p = 0.0013$) in liver sections of rats. Magnification of ×400 shows increased nuclear and cytoplasmic positive marks in the SRD group. Scale bar: 50 $\mu$m. Values (mean ± SEM, $n = 6$) are expressed as integrated optical density (IOD). **g** Densitometric immunoblot analysis of the $CB_2R$ protein mass levels ($p = 0.0090$). Each gel contained an equal number of samples from rats fed a RD, SRD, and SRD + CO. Values are expressed as mean ± SEM ($n = 6$). Bars that do not share the same letter are significantly different ($p < 0.05$) by one-way ANOVA followed by the Newman-Keuls test.

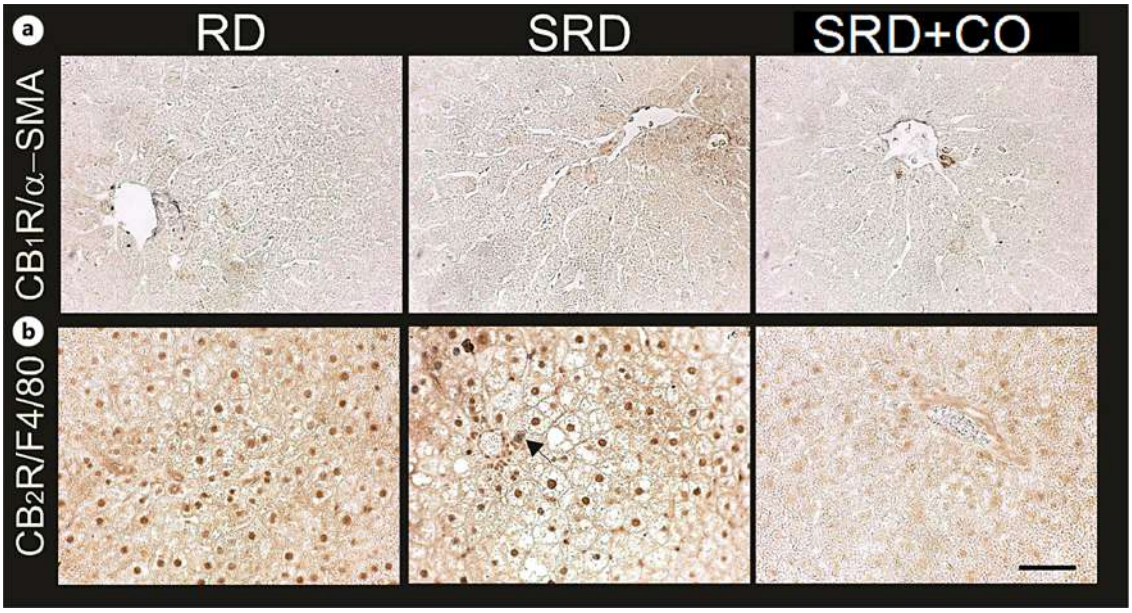


**Fig. 4.** Double-labeling immunohistochemistry suggests partial distribution of $CB_1R$ in α-smooth muscle actin-positive cells and $CB_2R$ in F4/80-positive cells in SRD livers, while cannabis oil prevented these changes. **a** Representative photomicrographs of double-labeling immunohistochemistry for CB1R/α-smooth muscle actin (α-SMA) in liver sections. **b** Representative photomicrographs of double-labeling immunohistochemistry for $CB_2R$/F4/80 in liver sections from the same experimental groups. $CB_1R$ and $CB_2R$ immunoreactivity are visualized in brown (DAB), whereas α-SMA and F4/80 are detected in black. Black arrow: F4/80-positive cells. Scale bar: 50 $\mu$m.

stromal fibrosis. Although ultrastructural studies of cannabinoid effects in the liver are scarce, similar mitochondrial and structural protection has been reported in other tissues [53] and in studies of oxidative stress and fibrosis [13, 51, 55]. Importantly, an extensive literature search revealed no previous TEM-based demonstration of hepatic ultrastructural protection by full-spectrum CBD:THC formulations in sucrose-induced MASLD models, highlighting the novelty of our findings.

Together, our results support a model in which short-term sucrose intake induces metabolic stress, metainflammation, endothelial dysfunction, and early fibrosis, accompanied by increased hepatic $CB_1R$ and $CB_2R$ protein levels. In this context, $CB_1R$ upregulation may contribute to the progression of these alterations, whereas the increase in $CB_2R$ may be associated with the immune/inflammatory component triggered by SRD-induced liver injury. Daily CO administration prevented the SRD-induced increase in both receptors, in parallel with the attenuation of inflammation and tissue damage [20, 21, 48, 56, 57].

To further explore the cellular context of these changes, double-labeling immunohistochemistry was performed. $CB_1R$ signal showed partial co-localization with α-actin-positive cells, supporting its association with activated HSCs, in line with previous reports linking $CB_1R$ to fibrogenesis [21, 58]. In parallel, $CB_2R$ expression is partially co-localized with F4/80-positive cells, suggesting an association with immune cell populations [59, 60]. However, the limited macrophage abundance observed in this early-stage model indicates that the increase in $CB_2R$ cannot be attributed solely to immune cell infiltration. Instead, these findings suggest that $CB_2R$ upregulation may reflect, at least in part, the hepatic inflammatory environment. Importantly, CO administration prevented the SRD-induced increase in $CB_1R$ and $CB_2R$ immunoreactivity, in agreement with its protective effects against fibrogenic and inflammatory alterations.

In parallel, the CBD:THC 2:1 oil appears to counteract metainflammatory signaling by restoring $CB_2R$ expression, attenuation of $CB_1R$ upregulation, and preserving cellular structure and microvascular homeostasis. Compared with isolated cannabinoids or selective $CB_1R$ antagonists, full-spectrum formulations appear to exert broader and more synergistic actions, likely driven by the entourage effect [61].

From a translational standpoint, two implications emerge: (1) sucrose overload alone – even in the absence of high dietary fats – is sufficient to trigger early MASLD

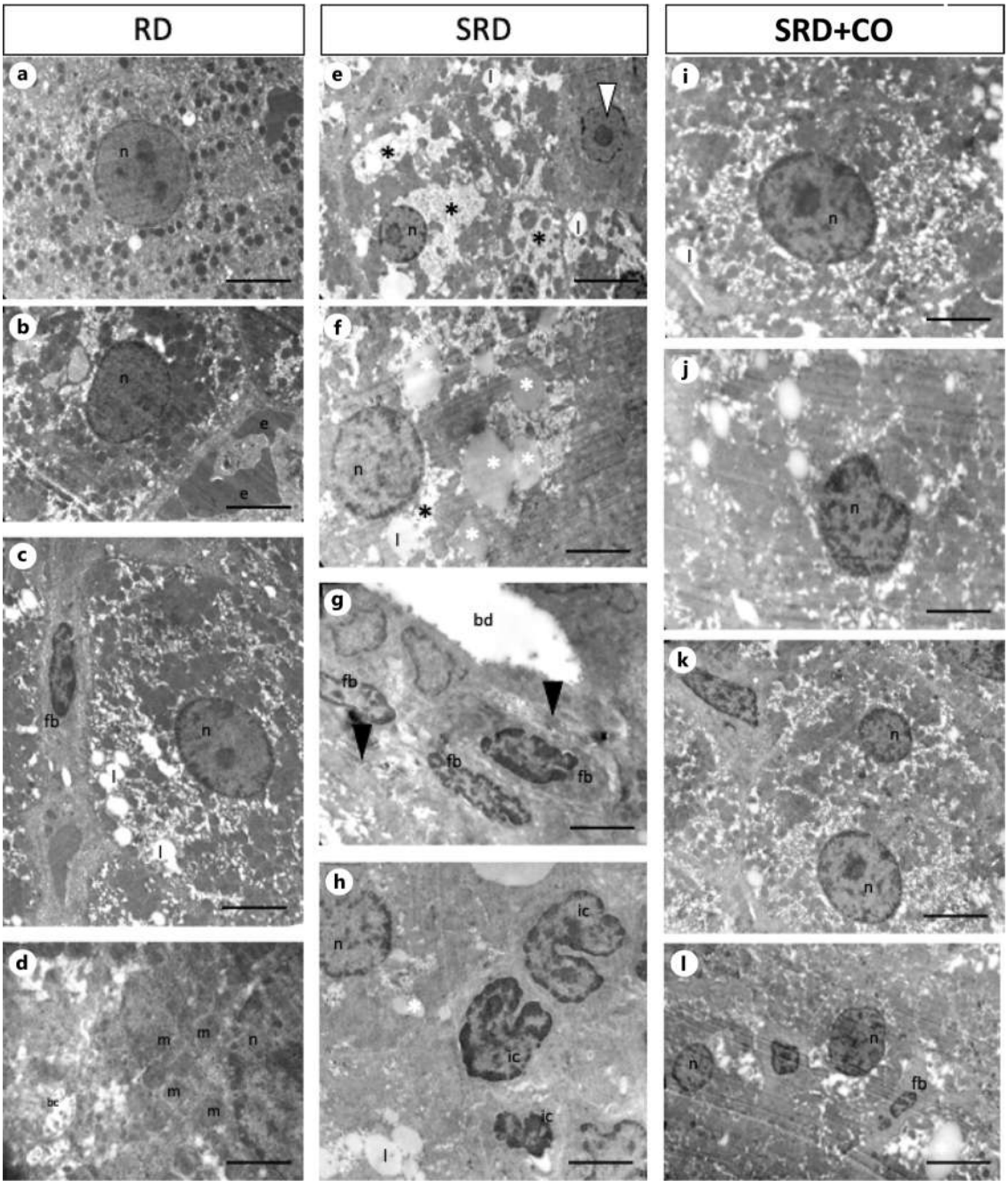


**Fig. 5.** SRD induced early ultrastructural liver alterations, while daily cannabis oil administration preserved hepatic architecture and reduced tissue damage. TEM images show nuclear irregularities, reduced mitochondrial content, and increased lipid and glycogen accumulation, together with stromal fibrosis and inflammatory infiltration in SRD-fed rats. In contrast, SRD + CO rats displayed preserved nuclear and mitochondrial morphology and reduced lipid and glycogen deposits. n, hepatocyte nuclei; bc, biliary canalicule; bd, biliary duct; ic, inflammatory cell; fb, fibroblast; e, erythrocytes; l, lysosome. White arrow: apoptotic nuclei; black arrow: collagen deposit; white asterisk: lipid droplet; black asterisk: glycogen accumulation. Scale bars: **a**, **b**, **c**, **f**, **g**, **h**, **i**, **j**, **k** = 4 μm; **d** = 0.5 μm; **e**, **l** = 1 μm.

features, reinforcing the critical importance of reducing refined sugar intake; (2) phytocannabinoid combinations represent promising multi-target therapeutic strategies capable of counteracting interconnected pathogenic mechanisms. Future work should investigate dose-response effects, long-term safety, the contribution of terpenes, and interactions with lifestyle interventions or emerging MASLD therapies.

The present study was designed to evaluate the preventive effects of daily CO administration during the early stages of SRD-induced MASLD. Because CO administration in the SRD + CO group began concomitantly with SRD exposure, the present findings should be interpreted within a preventive context.

Although an RD + CO group was not included in the full experimental design of the present study, preliminary observations obtained during the initial stages of the project showed no significant differences between RD and RD + CO animals in general parameters, including serum metabolites, liver injury enzyme activity, blood pressure, and the cannabinoid tetrad. These findings support the interpretation that the effects described here are primarily related to the prevention of SRD-induced alterations rather than to nonspecific actions of the oil under basal dietary conditions.

Another relevant aspect to consider is the potential contribution of intestinal mechanisms to the effects observed in the present study. The gut-liver axis plays an important role in MASLD development since alterations in intestinal permeability, microbial-derived products, and inflammatory signaling may contribute to hepatic steatosis, inflammation, and disease progression. In parallel, the ECS is an important regulator of gastrointestinal physiology, including intestinal motility, mucosal integrity, immune responses, and epithelial barrier function. Previous studies have shown that cannabinoid signaling can modulate gastrointestinal motility and intestinal permeability and that intestinal epithelial CB1R activation may impair barrier integrity through mechanisms involving tight junction protein regulation. In particular, activation of the intestinal epithelial CB1R-ERK1/2 pathway has been associated with downregulation of tight junction proteins and reduced villus length, while other dietary models have shown that CB1R participates in the regulation of intestinal permeability under metabolic stress conditions. Although these findings cannot be directly extrapolated to the present SRD model, they support the hypothesis that SRD-induced ECS alterations may also involve intestinal mechanisms. Considering that CO was administered orally, it is plausible that modulation of intestinal motility and/or epithelial barrier function could contribute, at least in part, to the hepatic effects observed in SRD + CO animals. However, intestinal permeability, gastrointestinal motility, microbiota composition, tight junction proteins, villus morphology, and endotoxemia-related markers were not evaluated in the present experimental design. Therefore, no direct conclusions can be drawn regarding the contribution of intestinal changes to the protective effects of CO in this model. Future studies should specifically assess these parameters to determine whether modulation of the gut-liver axis contributes to the preventive effects of orally administered CBD:THC 2:1 CO in SRD-induced MASLD [62–65].

Future studies using a therapeutic design, in which treatment is initiated after the metabolic and hepatic phenotype has been established, will be necessary to determine whether the CO is also able to reverse already established alterations. In this context, early markers of endothelial activation such as VCAM-1 may represent translationally relevant endpoints.

## Conclusion

Short-term sucrose overload was sufficient to trigger the earliest hallmarks of MASLD – including hepatic steatosis, metabolic inflammation, endothelial dysfunction, oxidative stress, and incipient fibrogenesis – in parallel with increased hepatic $CB_1R$ and $CB_2R$ protein levels. While $CB_1R$ upregulation may contribute to the progression of these alterations, increased $CB_2R$ levels may be linked to the immune/inflammatory response associated with liver injury. Daily CO administration prevented these alterations and the SRD-induced increase in cannabinoid receptor protein levels. Ultrastructural analyses further confirmed these hepatoprotective effects by revealing preserved nuclear and mitochondrial integrity, reduced lipid and glycogen accumulation, and absence of stromal fibrosis or inflammatory infiltrates.

These findings position ECS modulation – particularly through phytocannabinoid combinations – as a promising multi-target strategy capable of mitigating the earliest pathogenesis processes underlying MASLD. The induction of MASLD features induced by sucrose alone emphasizes the urgency of limiting refined sugar intake as primary preventive measure. Future studies should explore dose-response dynamics, long-term efficacy and safety, and the contribution of terpenes and other bioactive components, as well as evaluate the integration of

phytocannabinoid-based therapies with lifestyle and emerging pharmacological interventions to facilitate their clinical translation.


## Acknowledgments

The authors would like to thank Michelle Berenice Vega Joubert and Cristian Vaccarini for their skillful technical assistance.


## Statement of Ethics

This study was performed in strict accordance with the NIH guidelines for the care and use of laboratory animals and approved by the Institutional Ethics Committee of the Faculty of Biochemistry and Biological Sciences (UNL, Santa Fe, Argentine – Acta 03/21).

## Conflict of Interest Statement

The authors declare that there is no conflict of interest.


## Funding Sources

This work was supported by Agencia Santafesina de Ciencia, Tecnología e Innovación from Argentina (PEICID-2021-003).


## Author Contributions

Valentina Degrave and Paola Ingaramo: investigation, data curation, formal analysis, and writing the manuscript. Laura Caltana: investigation, methodology, data curation, formal analysis, and writing the manuscript. Daniela Sedan and Dario Andrinolo: investigation, data curation, and formal analysis. María Eugenia D'Alessandro: conceptualization, methodology, data curation, formal analysis, and writing the manuscript. María Eugenia Oliva: funding acquisition, conceptualization, investigation, methodology, data curation, formal analysis, supervision, and writing the manuscript.

## Data Availability Statement

All data generated or analyzed during this study are included in this article. Further inquiries can be directed to the corresponding author.

## References


1 Chan WK, Chuah KH, Rajaram RB, Lim LL, Ratnasingam J, Vethakkan SR. Metabolic dysfunction-associated steatotic liver disease (MASLD): a state-of-the-art review. J Obes Metab Syndr. 2023;32(3):197–213. https://doi.org/10.7570/jomes23052

2 Stefan N, Yki-Järvinen H, Neuschwander-Tetri BA. Metabolic dysfunction-associated steatotic liver disease: heterogeneous pathomechanisms and effectiveness of metabolism-based treatment. Lancet Diabetes Endocrinol. 2025;13(2):134–48. https://doi.org/10.1016/s2213-8587(24)00318-8

3 Parisse S, Coltorti E, Mischitelli M, Ferri F, Ginanni Corradini S. New insights into the interplay between simple sugars and liver diseases. Curr Issues Mol Biol. 2025;47(6):390. https://doi.org/10.3390/cimb47060390

4 Rossi AS, Oliva ME, Ferreira MR, Chicco A, Lombardo YB. Dietary chia seed induced changes in hepatic transcription factors and their target lipogenic and oxidative enzyme activities in dyslipidaemic insulin-resistant rats. Br J Nutr. 2013;109(9):1617–27. https://doi.org/10.1017/s0007114512003558

5 Degrave V, Vega Joubert MB, Filippa C, Ingaramo P, Torregiani L, Caro YS, et al. Effects of five cannabis oils with different CBD:THC ratios and terpenes on hypertension, dyslipidemia, hepatic steatosis, oxidative stress, and CB1 receptor in an experimental model. J Cannabis Res. 2025;7(1):46. https://doi.org/10.1186/s42238-025-00286-8

6 Dewidar B, Meyer C, Dooley S, Meindl-Beinker AN. TGF-β in hepatic stellate cell activation and liver fibrogenesis. Cells. 2019;8(11):1419. https://doi.org/10.3390/cells8111419

7 Horn P, Tacke F. Metabolic reprogramming in liver fibrosis. Cell Metab. 2024;36(7):1439–55. https://doi.org/10.1016/j.cmet.2024.05.003

8 Zhou IY, Clavijo Jordan V, Rotile NJ, Akam E, Krishnan S, Arora G, et al. Advanced MRI of liver fibrosis and treatment response in a rat model of nonalcoholic steatohepatitis. Radiology. 2020;296(1):67–75. https://doi.org/10.1148/radiol.2020192118

9 Oliva ME, Ingaramo P, Vega Joubert MB, Ferreira MR, D'Alessandro ME. Blood coagulation, endothelial dysfunction and liver fibrosis study in an experimental model of metabolic syndrome: effects of Salvia hispanica L. (chia) seed. Food Funct. 2021;12(24):12407–20. https://doi.org/10.1039/d1fo02274a

10 Pellicano AJ, Spahn K, Zhou P, Goldberg ID, Narayan P. Collagen characterization in a model of nonalcoholic steatohepatitis with fibrosis: a call for development of targeted therapeutics. Molecules. 2021;26(11):3316. https://doi.org/10.3390/molecules26113316

11 Amer MA, Othman AI, El-Missiry MA, Farag AA, Amer ME. Proanthocyanidins attenuated liver damage and suppressed fibrosis in CCl4-treated rats. Environ Sci Pollut Res. 2022;29(60):91127–38. https://doi.org/10.1007/s11356-022-22051-7

12 Nesci A, Ruggieri V, Manilla V, Spinelli I, Santoro L, Di Giorgio A, et al. Endothelial dysfunction and liver cirrhosis: unraveling of a complex relationship. Int J Mol Sci. 2024;25(23):12859. https://doi.org/10.3390/ijms252312859

13 Dai Q, Ain Q, Seth N, Rooney M, Zipprich A. Liver sinusoidal endothelial cells: friend or foe in metabolic dysfunction-associated steatotic liver disease/metabolic dysfunction-associated steatohepatitis. Dig Liver Dis. 2025;57(5):943–53. https://doi.org/10.1016/j.dld.2025.01.189

14 Rafaqat S, Gluscevic S, Mercantepe F, Rafaqat S, Klisic A. Interleukins: pathogenesis in non-alcoholic fatty liver disease. Metabolites. 2024;14(3):153. https://doi.org/10.3390/metabo14030153

15 Solleiro-Villavicencio H, Viurcos-Sanabria R, Aguayo-Guerrero JA, Pineda-Pérez PF, Méndez-García LA. Inflammation: a key mechanism connecting metabolic-associated steatotic liver disease and systemic arterial hypertension. Front Immunol. 2025;16:1620585. https://doi.org/10.3389/fimmu.2025.1620585

16 Vachliotis ID, Polyzos SA. The intriguing roles of cytokines in metabolic dysfunction-associated steatotic liver disease: a narrative review. Curr Obes Rep. 2025;14(1):65. https://doi.org/10.1007/s13679-025-00657-5

17 Tam J, Liu J, Mukhopadhyay B, Cinar R, Godlewski G, Kunos G. Endocannabinoids in liver disease. Hepatology. 2011;53(1):346–55. https://doi.org/10.1002/hep.24077
18 Di Marzo V, Silvestri C. Lifestyle and metabolic syndrome: contribution of the endocannabinoidome. Nutrients. 2019;11(8):1956. https://doi.org/10.3390/nu11081956
19 Simankowicz P, Stępniewska J. The role of endocannabinoids in physiological processes and disease pathology: a comprehensive review. J Clin Med. 2025;14(8):2851. https://doi.org/10.3390/jcm14082851
20 Chen S, Kim JK. The role of cannabidiol in liver disease: a systemic review. Int J Mol Sci. 2024;25(4):2370. https://doi.org/10.3390/ijms25042370
21 Parfieniuk-Kowerda A, Martonik D, Andrzejuk A, Tarasik A, Flisiak R. Cannabinoids and the endocannabinoid system in liver diseases. Clin Exp Hepatol. 2024;10(4):211–7. https://doi.org/10.5114/ceh.2024.145358
22 Degrave V, Vega Joubert MB, Ingaramo P, Sedan D, Andrinolo D, D'Alessandro ME, et al. Effects of full-spectrum cannabis oil with a cannabidiol:tetrahydrocannabinol 2:1 ratio on mechanisms involved in hepatic steatosis and oxidative stress in rats fed a sucrose-rich diet. Med Cannabis Cannabinoids. 2023;6(1):170–83. https://doi.org/10.1159/000534610
23 Hein GJ, Bernasconi AM, Montanaro MA, Pellon-Maison M, Finarelli G, Chicco A, et al. Nuclear receptors and hepatic lipidogenic enzyme response to a dyslipidemic sucrose-rich diet and its reversal by fish oil n-3 polyunsaturated fatty acids. Am J Physiol Endocrinol Metab. 2010;298(3):E429–39. https://doi.org/10.1152/ajpendo.00513.2009
24 Neuman RE, Logan MA. The determination of hydroxyproline. J Biol Chem. 1950;184(1):299–306. https://doi.org/10.1016/s0021-9258(19)51149-8
25 Creus A, Benmelej A, Villafañe N, Lombardo YB. Dietary Salba (Salvia hispanica L.) improves the altered metabolic fate of glucose and reduces increased collagen deposition in the heart of insulin-resistant rats. Prostaglandins Leukot Essent Fatty Acids. 2017;121:30–9. https://doi.org/10.1016/j.plefa.2017.06.002
26 Altamirano GA, Delconte MB, Gomez AL, Ingaramo PI, Bosquiazzo VL, Luque EH, et al. Postnatal exposure to a glyphosate-based herbicide modifies mammary gland growth and development in wistar male rats. Food Chem Toxicol. 2018;118:111–8. https://doi.org/10.1016/j.fct.2018.05.011
27 Vega Joubert MB, Ingaramo P, Oliva ME, D'Alessandro ME, Salvia hispanica L. (chia) seed ameliorates liver injury and oxidative stress by modulating Nrf2 and NF-κB expression in sucrose-rich diet-fed rats. Food Funct. 2022;13:7333–45. https://doi.org/10.1039/d2fo00642a
28 Ingaramo PI, Alarcón R, Caglieris ML, Varayoud J, Muñoz-de-Toro MM, Luque EH. Altered uterine angiogenesis in rats treated with a glyphosate-based herbicide. Environ Pollut. 2022;296:118729–39. https://doi.org/10.1016/j.envpol.2021.118729
29 Ingaramo PI, Guerrero Schimpf M, Milesi MM, Luque EH, Varayoud J. Acute uterine effects and long-term reproductive alterations in postnatally exposed female rats to a mixture of commercial formulations of endosulfan and glyphosate. Food Chem Toxicol. 2019;134:110832. https://doi.org/10.1016/j.fct.2019.110832
30 Li W, Jiang L, Lu X, Liu X, Ling M. Curcumin protects radiation-induced liver damage in rats through the NF-κB signaling pathway. BMC Complement Med Ther. 2021;21(1):10. https://doi.org/10.1186/s12906-020-03182-1
31 Reynolds ES. The use of lead citrate at high pH as an electron-opaque stain in electron microscopy. J Cel Biol. 1963;17(1):208–12. https://doi.org/10.1083/jcb.17.1.208
32 Zhang Q, Jin Y, Xin X, An Z, Hu Y, Li Y, et al. A high-trans fat, high-carbohydrate, high-cholesterol, high-cholate diet-induced nonalcoholic steatohepatitis mouse model and its hepatic immune response. Nutr Metab. 2023;20(1):28. https://doi.org/10.1186/s12986-023-00749-w
33 Roncal-Jimenez CA, Lanaspa MA, Rivard CJ, Nakagawa T, Sanchez-Lozada LG, Jalal D, et al. Sucrose induces fatty liver and pancreatic inflammation in male breeder rats independent of excess energy intake. Metabolism. 2011;60(9):1259–70. https://doi.org/10.1016/j.metabol.2011.01.008
34 Muriel P, López-Sánchez P, Ramos-Tovar E. Fructose and the liver. Int J Mol Sci. 2021;22(13):6969. https://doi.org/10.3390/ijms22136969
35 Lodge M, Dykes R, Kennedy A. Regulation of fructose metabolism in nonalcoholic fatty liver disease. Biomolecules. 2024;14(7):845. https://doi.org/10.3390/biom14070845
36 Zhou X, Zhang X, Niu D, Zhang S, Wang H, Zhang X, et al. Gut microbiota induces hepatic steatosis by modulating the T-cell balance in high fructose diet mice. Sci Rep. 2023;13(1):6701. https://doi.org/10.1038/s41598-023-33806-8
37 Xiang M, Tian X, Wang H, Gan P, Zhang Q. Inappropriate diet exacerbates metabolic dysfunction-associated steatotic liver disease via abdominal obesity. Nutrients. 2024;16(23):4208. https://doi.org/10.3390/nu16234208
38 Rabbani N, Thornalley PJ. Molecular mechanisms of metabolic dysfunction-associated steatotic liver disease: functional analysis of glucose and fructose metabolism pathway. Clin Sci (Lond). 2025;139(21):1405–29. https://doi.org/10.1042/cs20257727
39 Zhang CY, Lu S, Yang M. Macrophage and inflammation in diabetes and metabolic dysfunction-associated steatotic liver disease: from mechanisms to therapeutic strategies. World J Diabetes. 2025;16(9):110515.
40 Julien B, Grenard P, Teixeira-Clerc F, Van Nhieu JT, Li L, Karsak M, et al. Antifibrogenic role of the cannabinoid receptor CB2 in the liver. Gastroenterology. 2005;128(3):742–55. https://doi.org/10.1053/j.gastro.2004.12.050
41 Turcotte C, Blanchet MR, Laviolette M, Flamand N. The CB2 receptor and its role as a regulator of inflammation. Cell Mol Life Sci. 2016;73(23):4449–70. https://doi.org/10.1007/s00018-016-2300-4
42 Nasiri-Ansari N, Androutsakos T, Flessa CM, Kyrou I, Siasos G, Randeva HS, et al. Endothelial cell dysfunction and nonalcoholic fatty liver disease (NAFLD): A Concise Review. Cells. 2022;12(11):2511. https://doi.org/10.3390/cells11162511
43 Theofilis P, Vordoni A, Nakas N, Kalaitzidis RG. Endothelial dysfunction in nonalcoholic fatty liver disease: a systematic review and meta-analysis. Life (Basel). 2022;12(5):718. https://doi.org/10.3390/life12050718
44 Furuta K, Guo Q, Pavelko KD, Lee JH, Robertson KD, Nakao Y, et al. Lipid-induced endothelial vascular cell adhesion molecule 1 promotes nonalcoholic steatohepatitis pathogenesis. J Clin Investig. 2021;131(6):e143690. https://doi.org/10.1172/jci143690
45 Yang Z, Zhao J, Xie K, Tang C, Gan C, Gao J. MASLD development: from molecular pathogenesis toward therapeutic strategies. Chin Med J Engl. 2025;138(15):1807–24. https://doi.org/10.1097/cm9.0000000000003629
46 Teixeira-Clerc F, Julien B, Grenard P, Van Nhieu JT, Deveaux V, Li L, et al. CB1 cannabinoid receptor antagonism: a new strategy for the treatment of liver fibrosis. Nat Med. 2006;12(6):671–6. https://doi.org/10.1038/nm1421
47 Mallat A, Teixeira-Clerc F, Lotersztajn S. Cannabinoid signaling and liver therapeutics. J Hepatol. 2013;59(4):891–6. https://doi.org/10.1016/j.jhep.2013.03.032
48 Rakotoarivelo V, Mayer TZ, Simard M, Flamand N, Di Marzo V. The impact of the CB2 cannabinoid receptor in inflammatory diseases: an update. Molecules. 2024;29(14):3381. https://doi.org/10.3390/molecules29143381
49 Yoon HH, Grimsey NL. Cannabinoid receptor 2 (CB2) in macrophages: a promising clinical target for immune disorders. Int J Mol Sci. 2025;26(17):8657. https://doi.org/10.3390/ijms26178657
50 Silvestri C, Di Marzo V. The endocannabinoid system in energy homeostasis and the etiopathology of metabolic disorders. Cel Metab. 2013;17(4):475–90. https://doi.org/10.1016/j.cmet.2013.03.001
51 Siegmund SV, Schwabe RF. Endocannabinoids and liver disease. II. Endocannabinoids in the pathogenesis and treatment of liver fibrosis. Am J Physiol Gastrointest Liver Physiol. 2008;294(2):G357–62. https://doi.org/10.1152/ajpgi.00456.2007

52 Mukhopadhyay P, Rajesh M, Horváth B, Bátkai S, Park O, Tanchian G, et al. Cannabidiol protects against hepatic ischemia/reperfusion injury by attenuating inflammatory signaling and response, oxidative/nitrative stress, and cell death. Free Radic Biol Med. 2011;50(10):1368–81. https://doi.org/10.1016/j.freeradbiomed.2011.02.021
53 Rajesh M, Mukhopadhyay P, Bátkai S, Haskó G, Liaudet L, Drel VR, et al. Cannabidiol attenuates high glucose-induced endothelial cell inflammatory response and barrier disruption. Am J Physiol Heart Circ Physiol. 2007;293(1):H610–9. https://doi.org/10.1152/ajpheart.00236.2007
54 Stanley CP, Wheal AJ, Randall MD, O'Sullivan SE. Cannabinoids alter endothelial function in the Zucker rat model of type 2 diabetes. Eur J Pharmacol. 2013;720(1–3):376–82. https://doi.org/10.1016/j.ejphar.2013.10.002
55 Huang C, Liang H, Liang X, Liu Y, Wang J, Jiang H, et al. The protective role of cannabidiol in stress-induced liver injury: modulating oxidative stress and mitochondrial damage. Front Pharmacol. 2025;16:1567210. https://doi.org/10.3389/fphar.2025.1567210
56 Lotersztajn S, Teixeira-Clerc F, Julien B, Deveaux V, Ichigotani Y, Manin S, et al. CB2 receptors as new therapeutic targets for liver diseases. Br J Pharmacol. 2008;153(2):286–9. https://doi.org/10.1038/sj.bjp.0707511
57 Eddin LB, Meeran MFN, Subramanya SB, Jha NK, Ojha S. Therapeutic potential of agents targeting cannabinoid type 2 receptors in organ fibrosis. Pharmacol Res Perspect. 2024;12(6):e1219. https://doi.org/10.1002/prp2.1219
58 Dai E, Zhang L, Ye L, Wan S, Feng L, Qi Q, et al. Hepatic expression of cannabinoid receptors CB1 and CB2 correlate with fibrogenesis in patients with chronic hepatitis B. Int J Infect Dis. 2017;59:124–30. https://doi.org/10.1016/j.ijid.2017.03.008
59 Louvet A, Teixeira-Clerc F, Chobert M, Deveaux V, Pavoine C, Zimmer A, et al. Cannabinoid CB2 receptors protect against alcoholic liver disease by regulating Kupffer cell polarization in mice. Hepatology. 2011;54(4):1217–26. https://doi.org/10.1002/hep.24524
60 Denaës T, Lodder J, Chobert MN, Ruiz I, Pawlotsky JM, Lotersztajn S, et al. The cannabinoid receptor 2 protects against alcoholic liver disease via a macrophage autophagy-dependent pathway. Sci Rep. 2016;6(1):28806. https://doi.org/10.1038/srep28806
61 Russo EB. The case for the entourage effect and conventional breeding of clinical cannabis: no "strain," no gain. Front Plant Sci. 2019;9:1969. https://doi.org/10.3389/fpls.2018.01969
62 Lee Y, Jo J, Chung HY, Pothoulakis C, Im E. Endocannabinoids in the gastrointestinal tract. Am J Physiol Gastrointest Liver Physiol. 2016;311(4):G655–66. https://doi.org/10.1152/ajpgi.00294.2015
63 Cuddihey H, Cavin JB, Keenan CM, Wallace LE, Vemuri K, Makriyannis A, et al. Role of CB1 receptors in the acute regulation of small intestinal permeability: effects of high-fat diet. Am J Physiol Gastrointest Liver Physiol. 2022;323(3):G219–38. https://doi.org/10.1152/ajpgi.00341.2021
64 Crowley K, Kiraga Ł, Miszczuk E, Skiba S, Banach J, Latek U, et al. Effects of cannabinoids on intestinal motility, barrier permeability, and therapeutic potential in gastrointestinal diseases. Int J Mol Sci. 2024;25(12):6682. https://doi.org/10.3390/ijms25126682
65 Maccioni L, Dvorácskó S, Godlewski G, Cinar R, Iyer MR, Gao B, et al. Gut cannabinoid receptor 1 regulates alcohol binge-induced intestinal permeability. eGastroenterology. 2025;3(1):e100173. https://doi.org/10.1136/egastro-2024-100173